DELAYED NEUTRONS

Farhad Dolatshahi, Dean C. Kaul, and Stephen D. Egbert
Science Applications International Corporation

When nuclear weapons explode, they produce neutrons in two groups characterized by their time of emission. Prompt neutrons emerge from fissioning atoms for a few microseconds following initiation of the explosion. Delayed neutrons emerge from fission products for several tens of seconds following the fissions. Because of this time difference, the two groups are produced in quite different materials. The prompt neutrons are produced within the still intact bomb; the delayed neutrons are produced within the fireball. The mass of the air in the fireball far exceeds the mass of the bomb material that is dispersed within it; thus the delayed neutrons are essentially produced in air. The difference in the materials in which the neutrons are produced requires different approaches in the calculation of the numbers that reach the survivors.

Nuclear bombs developed in recent years have been lighter than those dropped on Hiroshima and Nagasaki. Because of the smaller mass, relatively more prompt neutrons escape and they escape with higher energies. The number emerging is two orders of magnitude more than the number of delayed neutrons released. As a consequence, the delayed neutrons had been considered unimportant and no methods for calculating their penetration through the atmosphere had been developed. Because of the greater mass of the Hiroshima and Nagasaki bombs, the delayed neutrons could not be assumed to be negligible and the present work was initiated.

The delayed neutron program had three parts: 1) development of a computation method, 2) verification and validation of the method, and 3) calculation of the energy and angle-differential fluences for the Hiroshima and Nagasaki bombs and their incorporaion into the DS86 dosimetry program.

The Computation Method

The development of the computation method for delayed neutrons had three parts: 1) determination of the time and energy dependence of the delayed neutron emission, 2) determination of the time dependence of the air density around the fireball as it rose from the burst point, and 3) development of a transport calculation for air of nonuniform

Table 1. Delayed Neutron Time- and Energy-differential Distributions for Fast Fission of ^{235}U, ^{238}U, and ^{239}Pu

Nuclide	Half-Life Group	Half-Life (seconds)	Population		E (MeV)	Kt (MeV)
			per Fission	per Kt		
U-235	1	55.70	5.40−4[a]	7.92+19	0.201	0.134
($\bar{\nu}_d$=0.0198)	2	20.54	4.18−3	6.13+20	0.420	0.280
	3	4.680	3.91−3	5.74+20	0.396	0.264
	4	1.944	7.53−3	1.11+21	0.438	0.292
	5	0.533	2.84−3	4.17+20	0.410	0.273
	6	0.206	8.00−4	1.17+20	0.491	0.327
U-238	1	55.70	4.40−4	6.49+19	0.201	0.134
($\bar{\nu}_d$=0.0404)	2	21.87	6.32−3	9.32+20	0.457	0.304
	3	4.592	6.10−3	9.00+20	0.367	0.245
	4	1.740	1.75−2	2.58+21	0.426	0.284
	5	0.520	7.63−3	1.13+21	0.417	0.278
	6	0.203	2.38−3	3.51+20	0.498	0.332
Pu-239	1	55.70	1.90−4	2.70+19	0.201	0.134
($\bar{\nu}_d$=0.00724)	2	22.05	1.85−3	2.63+20	0.465	0.310
	3	4.920	1.35−3	1.92+20	0.359	0.239
	4	1.994	2.54−3	3.60+20	0.415	0.277
	5	0.576	1.13−3	1.60+20	0.415	0.277
	6	0.201	1.70−4	2.41+19	0.478	0.318

[a] Read as 5.40×10^{-4}.

density above a plane ground.

Delayed Neutron Emission. The published literature on delayed neutrons is concerned with production in nuclear reactors running at constant power levels. Bomb calculations require the numbers produced in a very short interval, which depend on a different weighting according to the half-lives of the emitting fission products. Table 1 summarizes our deductions from the most recent data from the Los Alamos National Laboratory (LANL) for steady-state reactors.[1]

The original data were listed by half-life of the emitter. They were divided into six groups with upper bounds on the half-life of 0.3, 0.8, 3, 9, 31, and ∞ seconds. The mean half-life in each group (third column in Table 1) is the mean weighted by the number of neutrons emitted. The number of neutrons per fission (fourth column) was converted to number per kt using the factors 1.467×10^{23} fissions per kt by neutrons of energies in the bomb for ^{235}U, 1.475×10^{23} for ^{238}U, and 1.419×10^{23} for ^{239}Pu;[2] the yield for ^{238}U was adjusted upward on the advice of LANL.[3]

Spectral data were provided in graphical form by LANL for ^{239}Pu (fast fission) in all six half-life groups. However, because delayed neutron emission is thermodynamic in nature it was postulated that the spectra could be well represented by a Maxwellian distribution having the average energy properties as specified for all isotopes by LANL. This was tried, tested as shown in Figure 1, and found to be satisfactory for the purpose of stipulating energy distributions by half-life group.

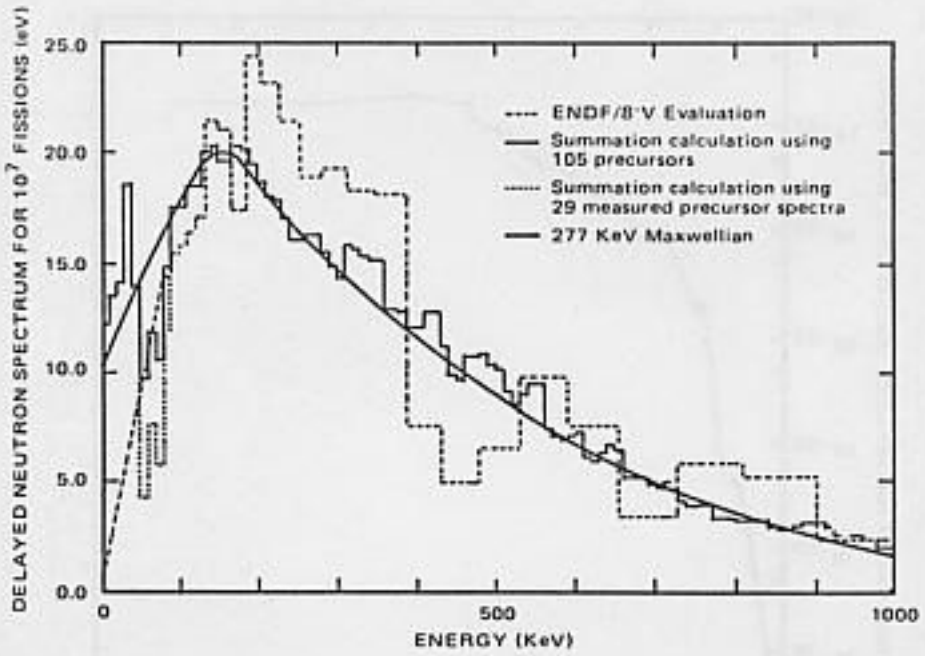

Figure 1. Comparison of ^{239}Pu (F) group 4 delayed neutron spectra

In summary, the delayed neutron source intensity is allowed to decrease from the time of burst according to the respective group half-life, with initial abundances according to the yield attributed to each fissionable nuclide. Spectra are stipulated separately for each fissionable nuclide and half-life group. This careful stipulation of spectra is important, because, as shown in Figure 2, the ability of source neutrons of energy E to produce kerma at 1100 m from the burst (in average, infinite, homogeneous Hiroshima air) drops rapidly in the region of the delayed neutron average energies. Thus, proper specification of the contribution of the high energy tail of the source is necessary to correctly calculate kerma values from transported delayed neutrons.

Air Density. Hydrodynamic models which are practical for use in computing air density profile between the rising fireball and some fixed point have been developed from a large data base of measurements on nuclear tests and detailed computer simulations. These models empirically scale data on the separate and interacting physical processes in order to describe the fluid mechanics of these detonations. The low altitude multiple burst (LAMB) model of Needham and Wittwer[4] is an example. It scales the hydrodynamic environment from a 1 kt standard burst and treats reflected shock by an image burst model. It also treats the fireball density well, buoyancy, air drag, reflected shock impulse, and focus information.

The LAMB model has been updated as new data have become available. The version of LAMB which is in NUIDEA,[5] an older code developed by SAIC to handle debris radiation computation applicable to antiballistic missile defense, has been used to generate the air density contours and line-of-sight air density profiles shown in Figures 3 and 4. The model recreates the density contours shown in Figure 3 and the line-of-sight to a detector location as shown in Figure 4. It is the latter type of data which is used to compute the transport of delayed neutron radiation, as will be described below.

The LAMB code has been modified independently by its users, ostensibly to improve

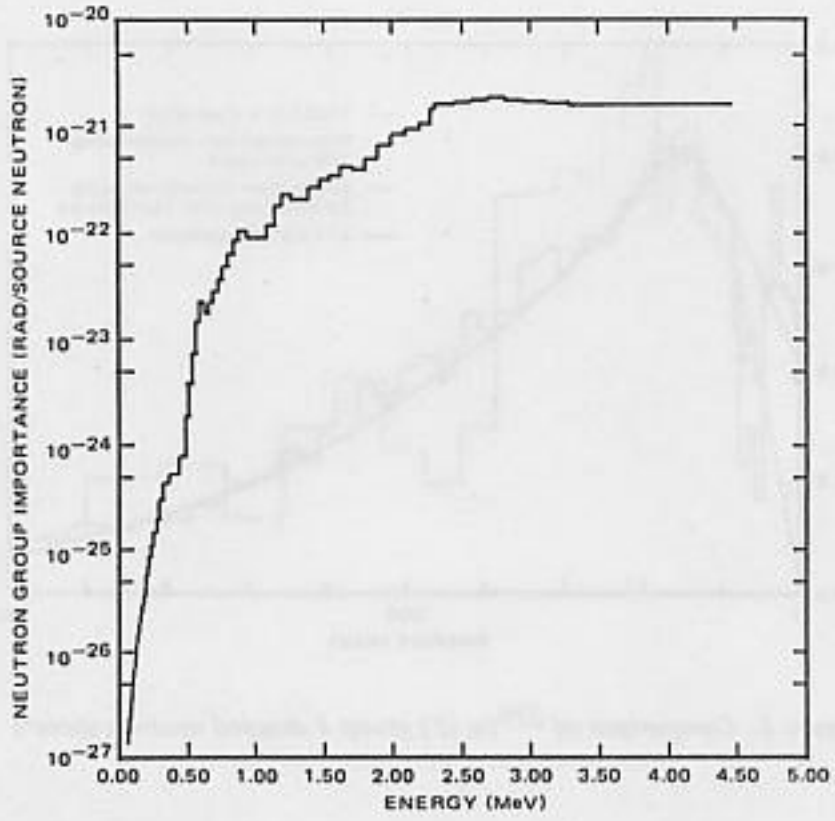

Figure 2. Neutron group importance in average Hiroshima-Nagasaki (infinite) air for production of kerma in tissue at a point in air near the ground at 1100 m slant range

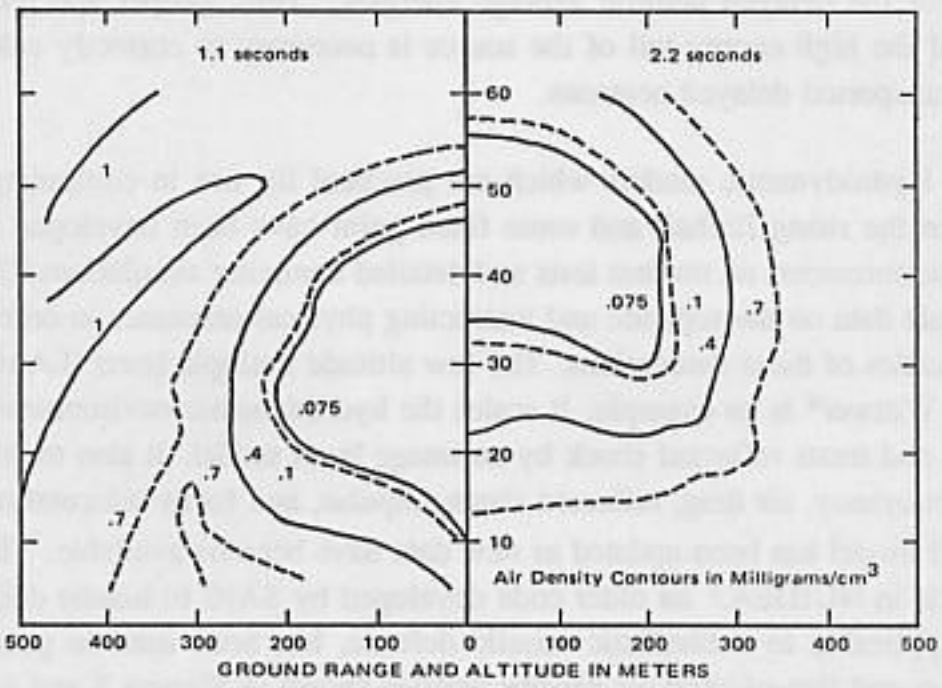

Figure 3. Two-dimensional profiles of the density of air computed with NUIDEA for Shot Plumbbob Owens (Yield 9.7 kt, height of burst 152 m) at 1.1 and 2.2 seconds after the burst

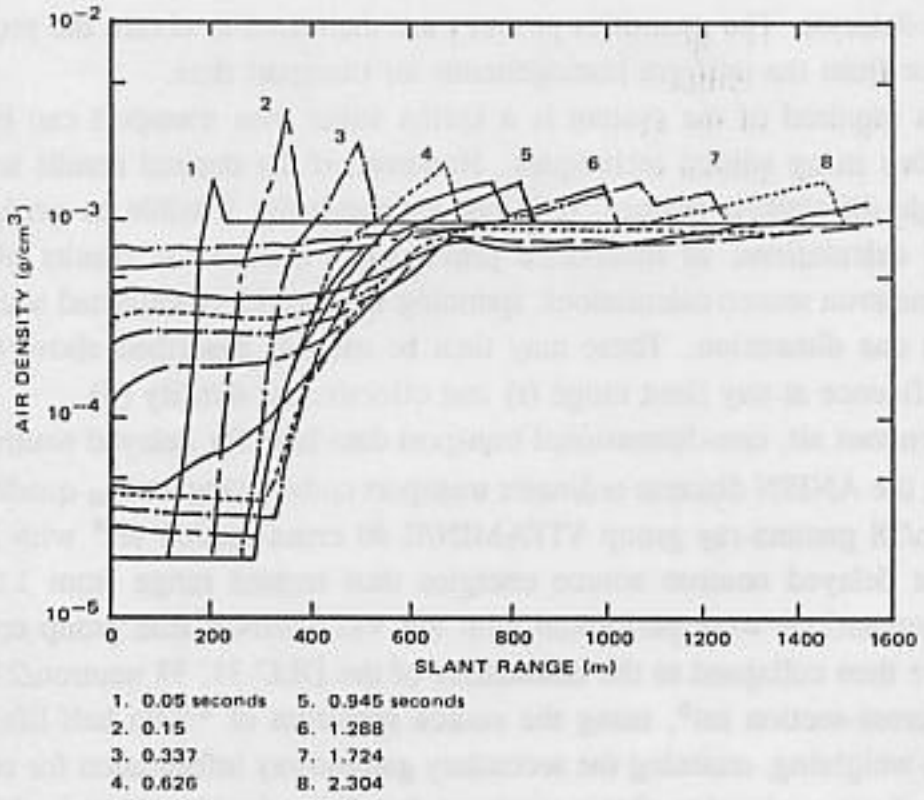

Figure 4. Line-of-sight density versus slant range and time as modeled by the LAMB model of the NUIDEA code for Shot Plumbbob Hood (yield 71 kt, height of burst 457 m)

certain aspects of its capabilities of particular interest for special applications. Dean[6] has modified the treatment of the density well in LAMB in the McDonnel-Douglas nuclear effects model STLAMB.

LAMB and STLAMB exhibit differences in the air mass integral along the detector line-of-sight, which controls radiation attenuation and, hence, dose. There are very few data which would allow any conclusion concerning choice of hydrodynamic models based on measured delayed neutron fluence or dose. Descriptions of calculation-measurement comparisons which can be performed will be described later. However, it is reasonable to assume that the delayed neutron and delayed gamma-ray models must use the same hydrodynamic model. And, because there are time dependent gamma-ray exposure rate measurements of delayed gamma rays at weapons tests, it is assumed that such data permit an adequate hydrodynamic model to be made. In the meantime the delayed neutron model described herein incorporates the STLAMB code.

Ideally, the transport of radiation from the time-dependent source through time-dependent air profiles should be performed in no less than two dimensions, incorporating detailed air density profiles as shown in Figure 3. However, this would require several hundred such calculations to describe the time dependence in sufficient detail. Therefore, such calculations have never been performed. Instead, transport has been performed in one or two dimensions using uniform air. The results are then scaled according to the line-of-sight air density profile to the detector at each time step (0.10 seconds). The scaling procedure requires that an integration be performed over the perturbed air along the line-of-sight air density profile to obtain the quantity (ρr) which is the equivalent to an average density times the actual slant

range (r) to the detector. The quantities ρr and r are then used to obtain the proper value of kerma or fluence from the uniform homogeneous air transport data.

If all that is required of the system is a kerma value then transport can be performed in two dimensions using adjoint techniques. However, if the desired results are to include energy and angle-differential fluence, it is not economically feasible to perform multiple two-dimenional calculations, as mentioned previously. Instead the results of a series of monoenergetic neutron source calculations, spanning the breadth of expected source energies, is performed in one dimension. These may then be used as described above to determine the differential fluence at any slant range (r) and effective air density (ρ).

The homogeneous air, one-dimensional transport data base for delayed neutrons has been generated using the ANISN discrete ordinates transport code[7] using an S_{40} quadrature set and the 174 neutron/38 gamma-ray group VITAMIN/E 40 cross-section set[8] with P_3 Legendre scattering. The delayed neutron source energies thus treated range from 1.07×10^{-5} to 4.72 MeV. Computations were performed with the VITAMIN/E fine group cross sections. The results were then collapsed to the boundaries of the DLC-31, 37 neutron/21 gamma-ray energy group, cross-section set[9], using the source spectrum of ^{239}Pu half-life group 4 for in-group source weighting, retaining the secondary gamma-ray information for completeness. This process has been repeated to obtain transport data bases for Hiroshima and Nagasaki air, as well as air having characteristics of such weapon tests as Shot Fox of Operation Ranger. These require separate data sets because of differences in air moisture content.

The VITAMIN/E cross sections were used for these calculations because the group boundaries of the DLC cross sections are much too broad in the region of greatest importance to delayed neutrons. The DLC-31 cross sections cause serious overprediction of the delayed neutron kerma as shown in Figure 5.

The effect of the ground on the transported neutrons is accounted for by performing an adjoint Monte Carlo calculation in which a detector is placed at the desired point above the ground, usually 1m. The adjoint fluence thus calculated, when convoluted with the one-dimensional forward fluence is capable of perturbing the latter for the presence of the ground, according to the expression:

$$\phi(E', \Omega') = \int_S \int_E \int_\Omega \phi(S, E, \Omega)\, \phi^*(S, E \rightarrow E',\ \Omega \rightarrow \Omega')\, n \cdot \Omega\, d\Omega\, dE\, dS \qquad (1)$$

where $\phi(E', \Omega')$ is the energy and angle-differential fluence perturbed for the presence of the ground, $\phi(S, E, \Omega)$ is the forward one-dimensional calculated fluence defined over a coupling surface S and ϕ^* is the adjoint fluence over that same surface, which correlates the energy and angle dependency of the incident fluence with that which exists at the detector location. This computation is performed using the VCS code system.[10]

The assumption of ρr scaling of uniform air results to account for hydrodynamic perturbations of air density works very well for photon transport, which is largely a line-of-sight affair. However, it does not work as well for neutrons, which can scatter through large angles without substantial energy loss, or of secondary gamma rays, which are born isotropically from neutron interactions.

The extent of deviation from uniform air scaling for delayed neutrons and secondary

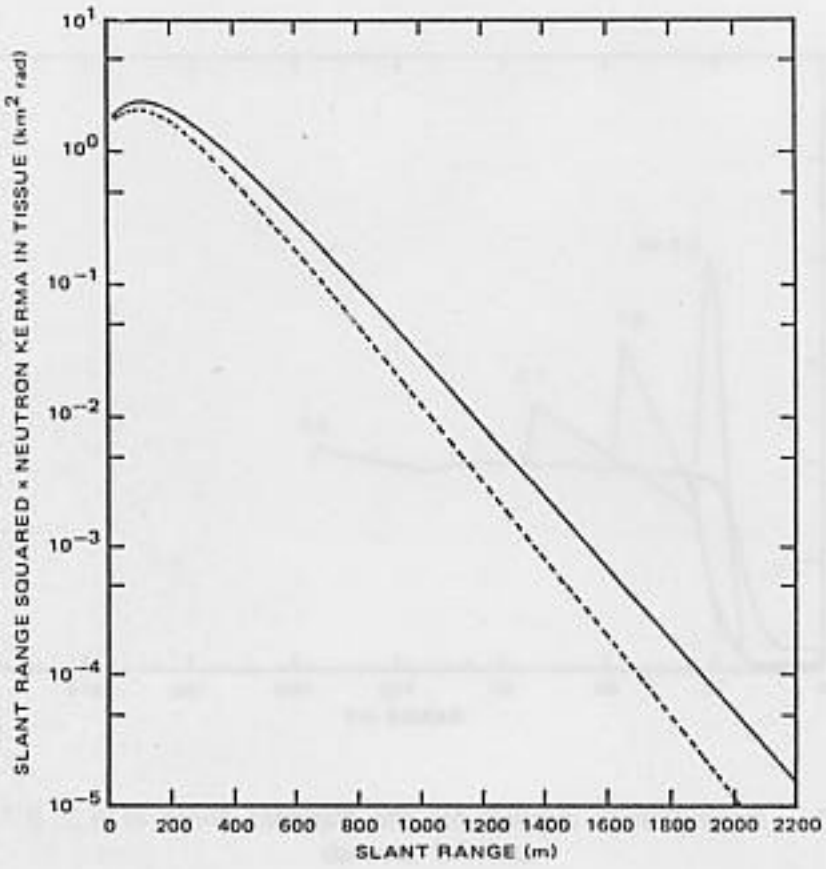

Figure 5. Typical delayed-neutron kerma in tissue at points in an infinite air mass having the average characteristics of Shot Ranger Fox

gamma rays from delayed nuetrons has been estimated using one-dimensional techniques. Coaltitude density profiles for the Nagasaki explosion were chosen at the midpoints of each period required to produce approximately one quarter of the total exposure at 1000 m. These were found to be 0.2, 0.7, 1.3, and 3.3 seconds. The resulting density profiles as obtained from STLAMB are shown in Figure 6. A representative delayed neutron source spectrum was placed at the center of the system and the transport to various ranges calculated for each profile using ANISN. An identical calculation in uniform air was then performed. The ratios of the four perturbed air kerma distributions to that in uniform air are shown in Figure 7.

The solid lines in Figure 7 depict the neutron kerma and the dashed lines depict the secondary gamma-ray kerma. The ratios are depicted as functions of ρr where ρ, the ambient density, has been given the arbitrary value of one atmosphere for the sake of simplicity. Note that for distance beyond the edge of the density well, a few hundred meters, the kerma in perturbed air are less than those for uniform air by a relatively consistent fraction. This is more true of the secondary gamma rays than the neutrons. However, using the data in Figure 7 to adjust the total delayed neutron fluence at various ranges one obtains the following perturbed-to-uniform air model ratios:

Range (m)	500	1000	1500	2000	2500
Ratio	0.83	0.63	0.64	0.66	0.71

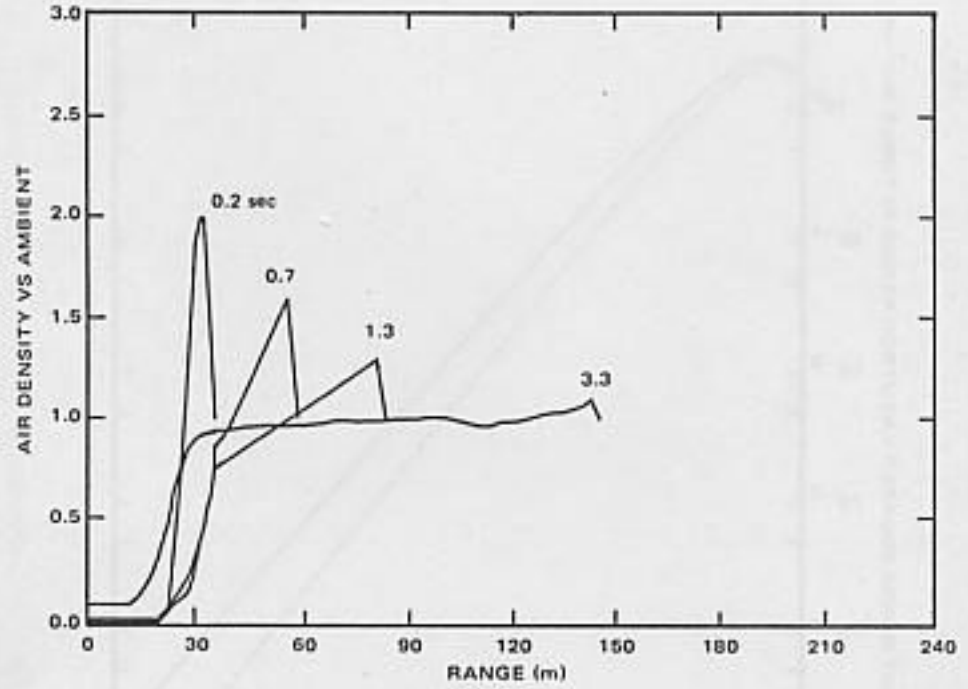

Figure 6. Range-density profiles for the Nagasaki bomb at 0.2, 0.7, 1.3, and 3.3 seconds

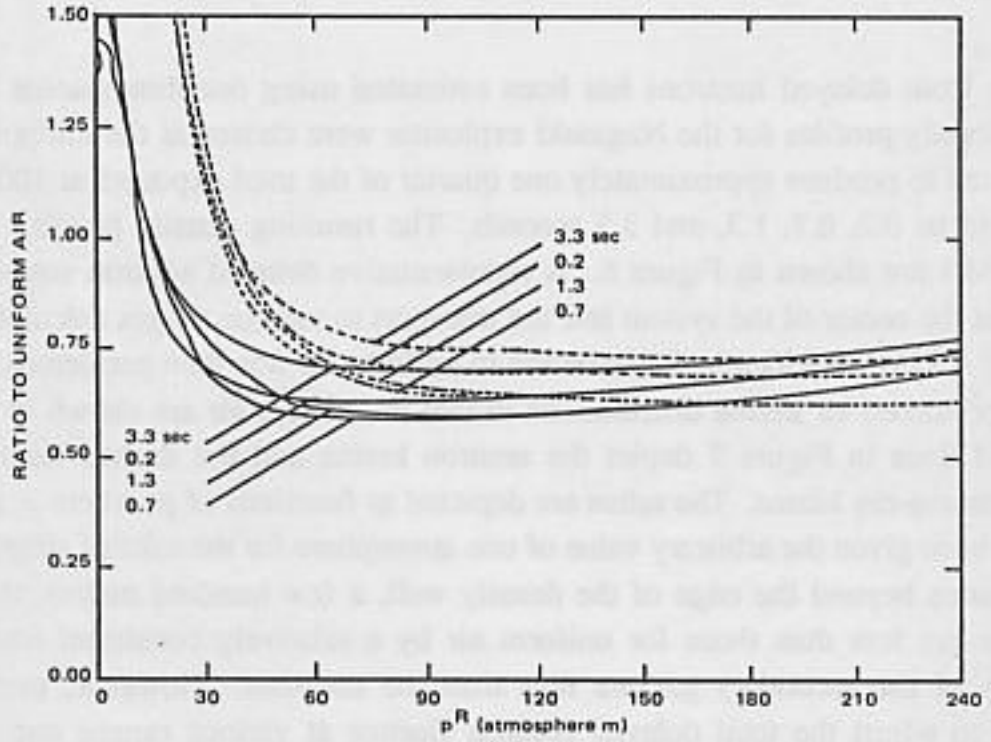

Figure 7. Delayed-neutron (solid line) and secondary gamma-ray kerma in tissue at points in hydrodynamically perturbed air relative to that in uniform air at 0.2, 0.7, 1.3, and 3.3 seconds for the Nagasaki bomb

For the present it was decided to take the value 0.667 as representative of the nonuniform air adjustment for delayed neutrons and secondary gamma rays for delayed neutrons. This is being done for all ranges, for yields in the range 10 to 30 kt, and for heights of burst sufficient to preserve the spherical fireball shape. This simplification seems justified given the course nature of the assessment, which does not account for any two-dimensional, yield, air moisture, or other effects. All results for delayed neutrons given in this paper have been adjusted using the 0.667 factor.

In summary the delayed neutron and secondary gamma-ray computation system calculates the propagation of neutron and secondary gamma rays in the form of energy and angle-differential fluence from a time and energy-differential source. The propagation is through uniform air scaled to account for hydrodynamic perturbations. Uniform air results are adjusted using a simple multiplicative factor to correct for errors in this approach. The results are corrected for the presence of the ground via forward-adjoint coupling, using the ground plane as a shielding medium. The results of this model are probably accurate to within a factor of two. Improvements will be incorporated as they become available.

Verification and Validation

Verification and validation of the delayed neutron model has been attempted using measured gold fluences at Shot Fox of Operation Ranger and Shot Dog of Operation Buster-Jangle, and the in situ cobalt activation measurements of Hashizume et al.[11]

Gold Fluence Measurements. Fluence below the cadmium cutoff (E = 0.414 eV) was calculated for Shot Fox. Ranger-Fox had a yield of 22 kt and was burst at a height of 436.47 ± 6 m. The bomb was air-dropped with lateral burst coordinates 107.16 m south and 196.14 m west of the normal Ranger aim point, uncertain to ±4.6 m. The meteorological specifications at shot time were reported as:

	Ground Level	Burst Height
Pressure (mb)	909	862
Temperature (°C)	−2.0	7.5
Relative humidity (%)	85	53
Dry air density (g/cm^3)	$1.162 \cdot 10^{-3}$	$1.063 \cdot 10^{-3}$
Moisture density (g/cm^3)	$3.588 \cdot 10^{-6}$	$4.256 \cdot 10^{-6}$
Total density (g/cm^3)	$1.166 \cdot 10^{-3}$	$1.067 \cdot 10^{-3}$

The foil line was laid out in a line due west, offset from the normal Ranger aim point 9.76 m south. The first foil was located 103.13 m west of a line running due south from the normal aim point. Subsequent foils were at 91.44 m intervals. All foil ranges were recalculated according to these data.

The upper energy bound of the DLC-31 thermal group is 0.414 eV, which is the effective value of the cadmium cutoff energy. The spectrum of thermal neutrons consistent with the use of DLC-31 cross sections is that of a 300° K Maxwellian distribution below 5 kt (0.129 eV) and a 1/E distribution between 0.129 E and 0.414 eV. The mean capture cross

section for gold weighted by such a spectral distribution is 78.5 barns. However, it is likely that the calibrations of the foils used at series Ranger and Buster were performed in water or graphite systems, having less energetic thermal spectra than that calculated using DLC-31 cross sections. It is assumed that the effective capture cross section for the calibration system is that for 2200 m/s neutrons (i.e., 99 barns). Thus the calculated thermal fluences for comparisons with test measurements have been multiplied by the ratio 78.5/99 in order to make them equivalent to the reported measurement values.

The results of gold foil measurements and calculations for Ranger-Fox are provided in Figures 8 and 9. The thermal neutrons contributed by the prompt component only are shown in Figure 8. It can be seen that the prompt thermal contribution changes slope abruptly at approximately 800 m slant range. This is due to the emergence of the high energy component from within the vast cloud of low energy (< 3 keV) neutrons caused by interactions with the thick high explosive material surrounding the device. The total calculated thermal neutron fluence distribution is shown together with the measured values in Figure 9. The agreement is generally improved beyond approximately 800 m with the addition of the delayed neutrons. However, the calculations appear to overestimate the gold fluence at close ranges.

Thermal fluences were also calculated for Buster-Jangle, shot Dog, a device very similar to Ranger-Fox. Buster-Dog had a yield of 21 kt and was burst at an altitude of 431.99 ± 3 m. Dog was air-dropped, having burst coordinates 17.1 m north and 11.0 m east of the aim point (± 4.6 m). The gold foil line started at Target 4 and ran on a line 48.82° × south of east, through Target 3 (the aim point) which was 293.49 m distant. Foils were at 91.44 m intervals with an extra foil at the aim point. All ranges from the burst point have been recalculated based on these data. The meteorological conditions at Buster-Dog were reported as:

	Ground Level	Burst Height
Pressure (mb)	876	832
Temperature (°C)	15.5	12
Relative humidity (%)	43	58
Dry air density (g/cm^3)	$1.048 \cdot 10^{-3}$	$1.007 \cdot 10^{-3}$
Moisture density (g/cm^3)	$5.700 \cdot 10^{-6}$	$6.191 \cdot 10^{-6}$
Total density (g/cm^3)	$1.054 \cdot 10^{-3}$	$1.013 \cdot 10^{-3}$

Because no radiation leakage data are currently available for Buster-Dog the transport results have been scaled from those of Ranger-Fox, although cloud rise and hydrodynamic conditions for Shot Dog were treated explicitly. Both events took place under relatively dry conditions. However, Buster-Dog had relatively more moisture in the air. Therefore, calculations shown here will represent an overestimate of the transmitted fluence to some degree.

The results of calculations and measurements fo cadmium-difference gold capture fluence 1 m above the ground are depicted in Figures 10 and 11. Figure 10 shows the calculated contribution from prompt neutrons. As in the case of Ranger-Fox the calculations using prompt thermals only underestimate the measured values beyond approximately 800 m. The

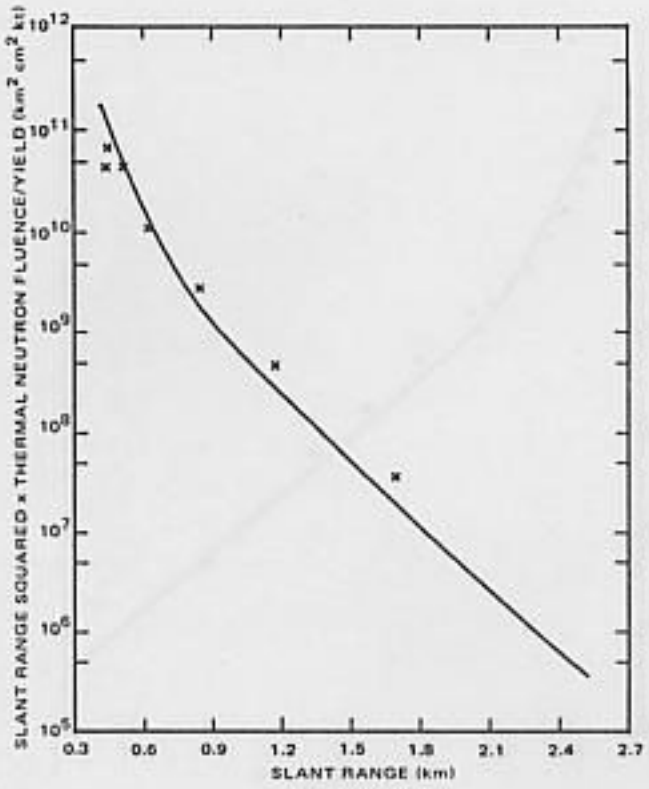

Figure 8. Comparison of gold-foil measurements with calculated fluence, per kt, for neutrons with velocity 2200 m/s. Prompt emission only. Shot Ranger Fox

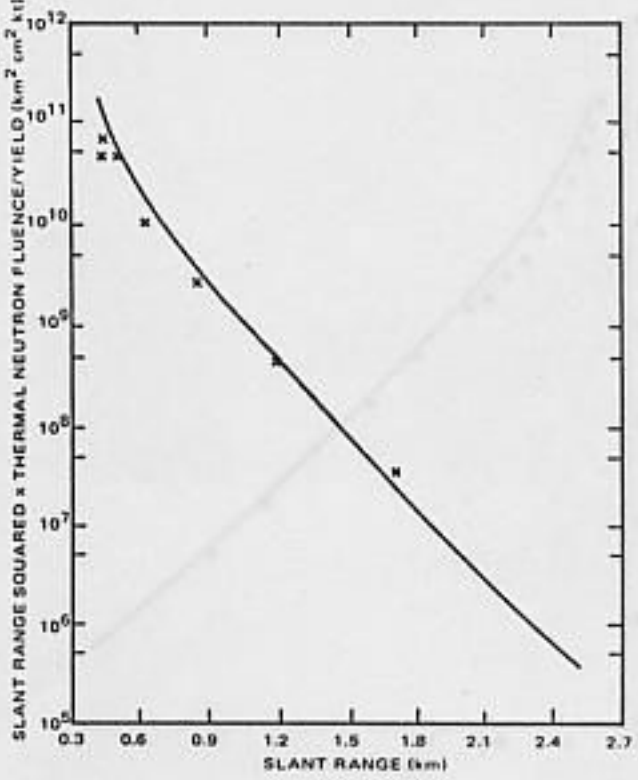

Figure 9. Comparison of gold-foil measurements with calculated fluence, per kt, for neutrons with velocity 2200 m/s. Prompt plus delayed emission. Shot Ranger Fox

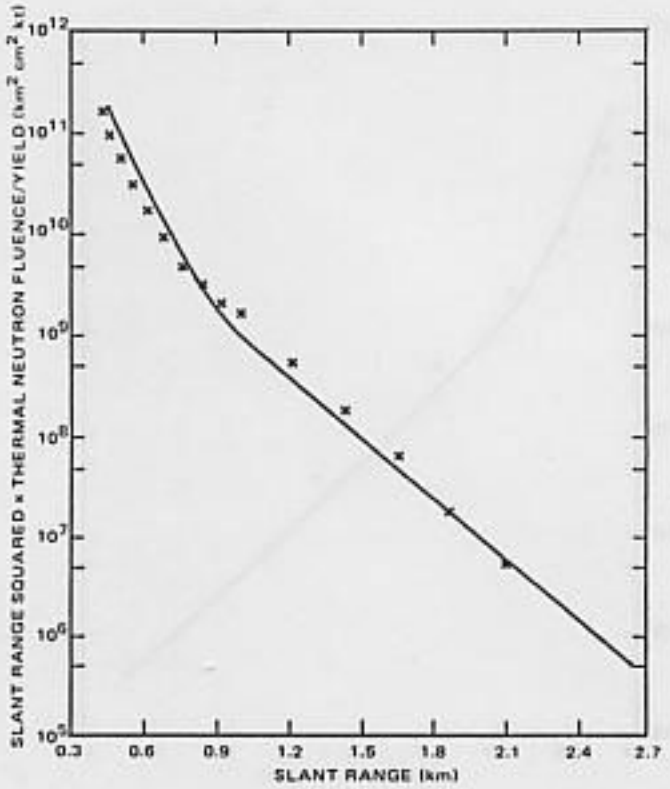

Figure 10. Comparison of gold-foil measurements with calculated fluence, per kt, for neutrons with velocity 2200 m/s. Prompt emission only. Shot BJ-Dog

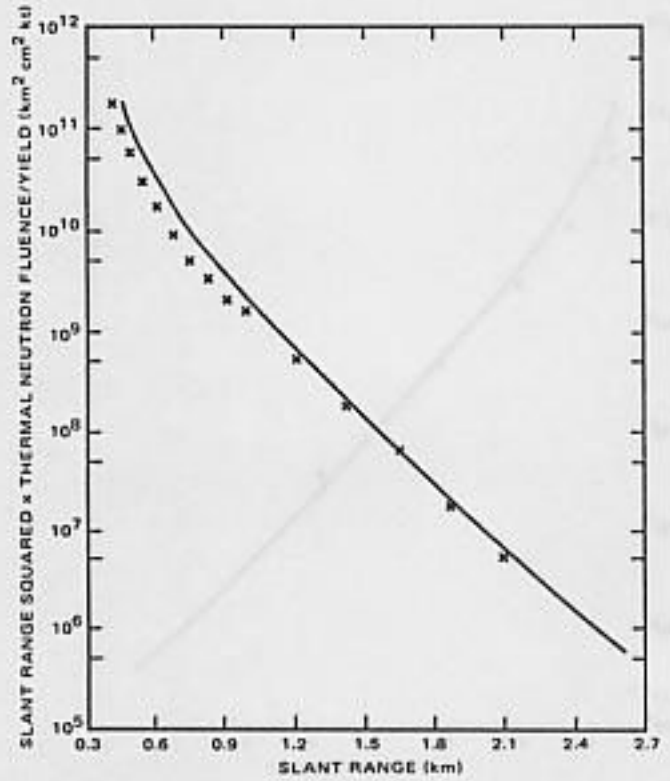

Figure 11. Comparison of gold-foil measurements with calculated fluence, per kt, for neutrons with velocity 2200 m/s. Prompt plus delayed emission. Shot BJ-Dog

Table 2. Concrete and Reinforcing Bar Constituents for Cobalt Activation Calculations (Joyama School Concrete).

	Concrete (g/cc)	Rebar (g/cc)
H	0.0142	
B	0.002 (0.001-0.003)	
C	0.0193	
O	1.2885	
Na	0.0442	
Mg	0.0198	
Al	0.1270	
Si	0.5951	
P	0.0016	
S	0.0025	
K	0.0320	
Ca	0.2071	
Cr	0.0005	
Mn	0.0015	
Fe	0.0623	7.87
Ni	0.0001	
	2.4200 g/cc (Range: 2.36-2.48)	7.87 g/cc

addition of the delayed component in Figure 11 improves agreement with the measured values at the longer ranges but makes it worse at shorter ranges.

Cobalt Activation. Activation of ^{59}Co in the reinforcing bars (rebar) of concrete structures was calculated to simulate the values measured by Hashizume et al.[11] Calculations were performed using the prompt neutron fields of Pace[12] and the delayed neutron fields as described in this report. Shielding was computed using the MORSE Monte Carlo code[13] and the VCS code system.[10]

The shielding calculations were performed for a rebar, 1 cm diameter, 8 cm deep in a concrete wall, and 1 m above the ground surface. The wall in which the rebar was imbedded was constituent to a building 10 × 10 × 10 m outer dimensions with 30 cm thick walls. The building and the paved ground surface surrounding the building were assumed to be made of the same concrete constituents as shown in Table 2. The building was surrounded to a height of 10 m with moist air corresponding to that at ground level at Hiroshima.[14] The air extended in a square to a distance of 50 m from the front of the building, 50 m from one side, and 40 m from the other side and the rear. The front face of the building was oriented as prescribed by Hashizume et al.[11]

The ^{59}Co activation cross-section set was taken from the VITAMIN/E library and collapsed to the DLC-31 neutron group structure using a 1/E spectrum with a Maxwellian below 0.414 eV.

The calculated and measured counts per minute per mg of ^{59}Co are given in Table 3. The calculations show a much steeper relaxation length than the measurements. This is qualitatively consistent with the finding of Loewe.[15]

Table 3. Cobalt Activation in Reinforcing Bar at Hiroshima and Nagasaki

Distance from Hypocenter (m)	Azimuth[a]	Activity cpm/mg Co				Δ%[b]
		Calculated			Measured	
		Prompt	Delayed	Total		
			Hiroshima			
260	10.44°	2.36+0[c]	1.34−1	2.50+0	2.09+0	+19.6
640	14.38°	2.17−1	1.75−2	2.34−1	3.24−1	−27.8
779	20.58°	7.28−2	6.35−3	7.92−2	1.46−1	−45.8
1180	8.10°	3.26−3	2.60−4	3.52−3	1.24−2	−71.6
			Nagasaki			
590	15.24°	4.88−2	4.97−2	9.85−2	1.40−1	−29.6
1030	19.19°	2.96−3	1.41−3	4.36−3	1.27−2	−65.7

[a]Angle between normal to wall and direction to Ground zero.
[b](Calc. − meas.) + meas. *100%.
[c]Read as 2.36*10° cpm/mg Co

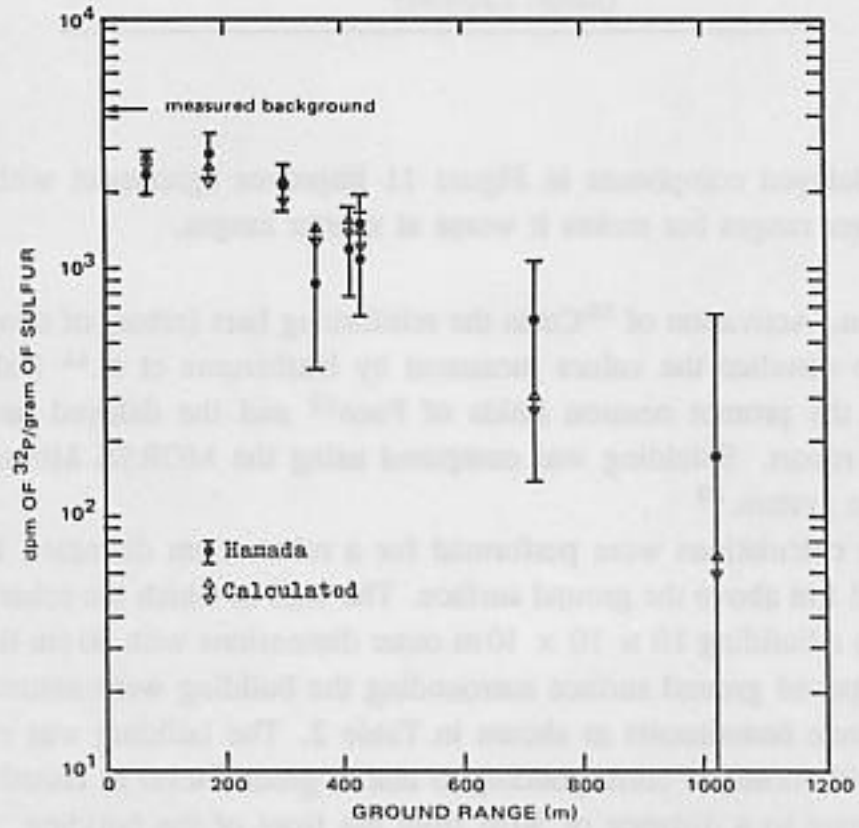

Figure 12. Comparison of measurements of ^{32}P induced in sulfur at Hiroshima with calculations.

According to the results of the Monte Carlo calculations the cobalt activation is caused by thermal and epithermal neutrons incident on the concrete. These are not in equilibrium with the fast neutrons at ranges of 1200 m or less. This is totally inconsistent with the measurements, which have a relaxation length characteristic of fast neutrons.

In looking for inconsistencies in the experimental data, which might explain the lack of agreement between calculation and measurement, only one was found. The uncertainty on the value quoted for Nagasaki at 1030 m (0.0127 ± 0.0010 pm/mg Co) was less than the quoted uncertainty on the background (0.069 ± 0.002). This discrepancy does not seem to aid materially in resolving the outstanding discrepancy.

In conclusion, regarding both the gold fluence and the cobalt activation, the calculated relaxation length is consistently too short. However, the two experiments imply different solutions to the problem. The test shot measurements indicate that the calculated values of the thermal fluence are much too large at close range and need to be reduced by on the order of a factor of two. The cobalt activation indicates that the fast neutron fluence should be increased to the point where its down scatter swamps the less energetic neutron transport from the device. This is hardly likely given the current results for Hiroshima sulphur activation as shown in Figure 12. It is more likely that, if the low energy neutrons are reduced at short range, the gold results will be in substantial agreement, relaxation length agreement, of calculated and measured cobalt activation will come more into agreement and that some other explanation will be found for the then more consistent descrepancy.

Delayed Neutron Fluence from the Bombs

The delayed neutron computation system, the development and testing of which have been described, has been used to calculate free-field fluence and kerma distributions from the Hiroshima and Nagasaki weapons. Calculations were performed using the mean atmospheric moisture-to-dry air ratio for the two cities, as follows.[14]

	Hiroshima	Nagasaki	Mean
Moisture/Dry Air	0.01591	0.01623	0.01607

Total hydrogen content in the soil was taken to be 3%, which is very similar to those in the revised ground specifications of Kerr,[16] which are 3.1% for Hiroshima and 3.5% for Nagasaki.

Results of calculations of delayed neutron and delayed neutron secondary gamma-ray propagation in terms of free-field kerma (rad in tissue) are provided for Hiroshima and Nagasaki in Tables 4 and 5. These tables also include the other free-field components. This is intended to put the delayed neutron components into perspective. Clearly, the secondary gamma rays from the delayed neutrons are a small fraction of the total, although that fraction increases slightly with range due to the relatively shorter relaxation length of the delayed gamma rays.

The delayed neutrons represent a significant fraction of the total neutron kerma at Nagasaki, 18% at 700 m, 11% at 1000 m, and over 4% at 1500 m. Perhaps more important, the delayed neutrons contribute an even larger number of neutrons at these ranges than their kerma implies, as evidenced by the cobalt activation results shown previously. Hiroshima, which already has a soft spectrum, gains more low energy neutrons from the delayed component. At Hiroshima the delayed neutron kerma is a smaller fraction of the total than at Nagasaki. However, because of the soft spectrum of prompt neutrons from the Hiroshima device, the delayed component remains a more consistent fraction with increasing range,

Table 4. Kerma (rad) Produced by Initial Radiation in Tissue at a Point in Air One meter Above the Ground at Hiroshima (15 kt Yield, 580 m Burst Height).

Distance from Hypocenter (m)	Neutron Kerma			Gamma-Ray Kerma			
					Delayed		
	Prompt	Delayed	Total	Prompt	1[a]	2[b]	Total
700	1.722+2[c]	9.793+0	1.820+2	5.414+2	9.247+2	1.432+1	1.480+3
1000	2.274+1	1.007+0	2.375+1	1.535+2	2.406+2	3.533+0	3.976+2
1300	3.082+0	9.367−2	3.176+0	4.723+1	6.314+1	1.607+0	1.114+2
1500	8.505−1	1.839−2	8.689−1	2.235+1	2.628+1	5.105−1	4.914+1
1700	2.439−1	3.760−3	2.477−1	1.076+1	1.132+1	2.543−1	2.233+1
2000	4.006−2	3.700−4	4.043−2	3.727+0	3.345+0	9.420−2	7.166+0

[a]Delayed gamma rays.
[b]Gamma rays from delayed neutrons.
[c]Read as 1.722×10^{2}.

Table 5. Kerma (rad) Produced by Initial Radiations in Tissue at a Point in Air One meter Above the Ground at Nagasaki (21 kt Yield, 503 m Burst Height).

Distance from Hypocenter (m)	Neutron Kerma			Gamma-Ray Kerma			
					Delayed		
	Prompt	Delayed	Total	Prompt	1[a]	2[b]	Total
700	8.249+1[c]	1.842+1	1.009+2	1.316+3	1.852+3	2.201+1	3.190+3
1000	1.310+1	1.685+0	1.479+1	3.614+2	4.327+2	4.641+0	7.987+2
1300	2.076+0	1.433−1	2.219+0	1.050+2	1.048+2	1.284+0	2.111+2
1500	6.213−1	2.764−2	6.489−1	4.833+1	4.247+1	6.007−1	9.140+1
1700	1.902−1	5.507−3	1.957−1	2.297+1	1.785+1	2.959−1	4.112+1
2000	3.364−2	5.136−4	3.415−2	7.853+0	5.063+0	1.068−1	1.302+1

[a]Delayed gamma rays.
[b]Gamma rays from delayed neutrons.
[c]Read as 8.249×10^{3}

going from 5.4% at 700 m to 0.9% at 2000 m. The transmitted spectra of delayed neutrons for Hiroshima and Nagasaki are shown in Figures 13 and 14 for four ranges. Note that because of the Maxwellian nature of the source the spectra are soft but with high energy tails extending to energies substantially above the mean source energy. In spite of this attention to detail it is expected that the delayed neutron fluence and kerma are overestimated at close ranges. Efforts are underway to understand the reason for this overestimate.

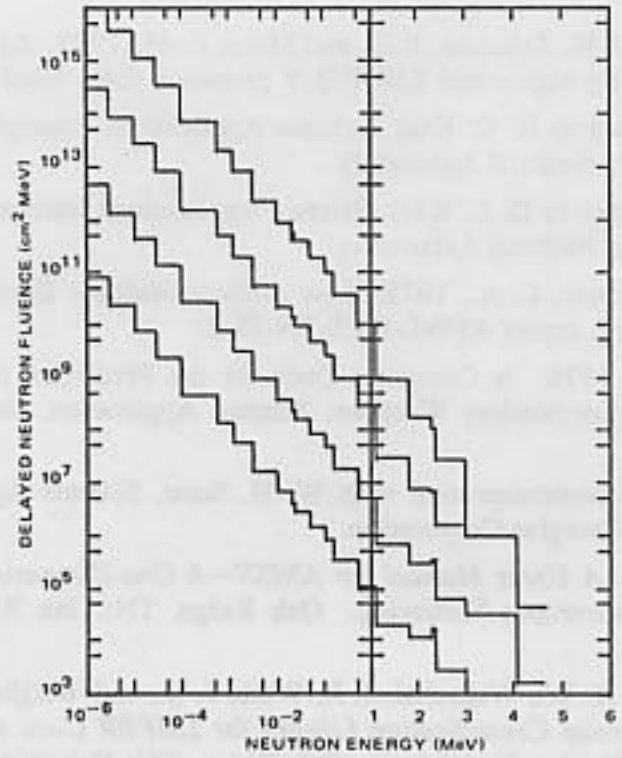

Figure 13. Delayed-neutron fluence distribution in energy for Hiroshima at 500, 1000, 1500, and 2000 m ground range

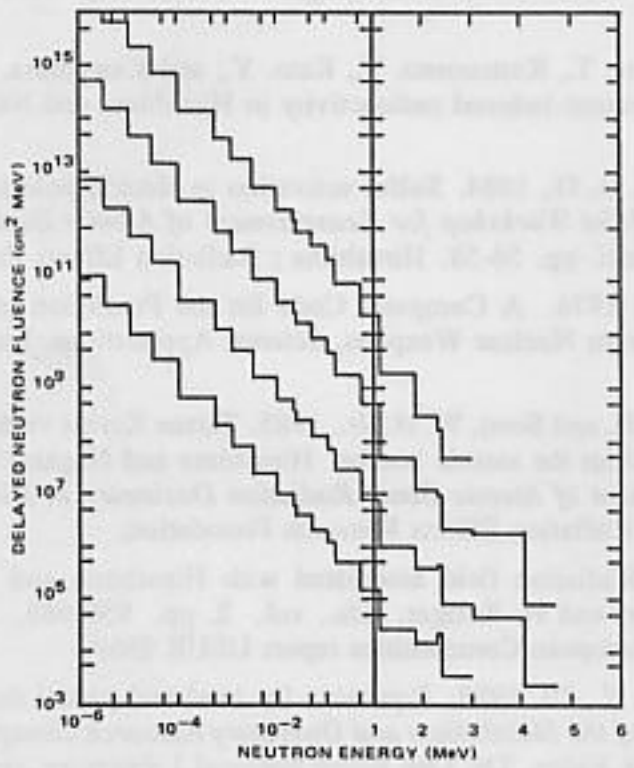

Figure 14. Delayed-neutron fluence distribution in energy for Nagasaki at 500, 1000, 1500, and 2000 m ground range

References

1. England, T. R., Wilson, W. B., Schenter, R.E., and Mann, F. M., 1983. Aggregate delayed neutron intensities and spectra using augmented ENDF/B-V precursor data. Nucl. Sci. Eng. 85:139-155.
2. Whalen, P. P., 1984. Letter to D. C. Kaul, Science Applications International Corporation. Los Alamos, NM: Los Alamos National Laboratory.
3. England, T. R., 1984. Letter to D. C. Kaul, Science Applications International Corporation. Los Alamos, NM: Los Alamos National Laboratory.
4. Needham, C. E. and Wittwer, L. A., 1975. *Low Altitude Multiple Burst (LAMB) Models.*, Air Force Weapons Laboratory, report AFWL-DYS-TN-75-2.
5. Straker E. A., Husar L., 1976. A Computer Code for the Prediction of Radiation, Blast, and Thermal Environments from Nuclear Weapons, Science Application, Incorporated Report SAI-76-851-LJ.
6. Dean, D., 1982. Private communication with W. H. Scott, Science Applications International Corporation. McDonnell-Douglas Corporation.
7. Engle, W. W., Jr., 1967. *A Users Manual for ANISN—A One-Dimensional Discrete Ordinates Transport Code With Anisotropic Scattering.* Oak Ridge, TN: Oak Ridge Gaseous Diffusion Plant, report K-1693.
8. Weisbin, C. R., Roussin, R. W., Wagschal, J. J., White J. E., and Wright, R. Q., 1979. *Vitamin-E: An ENDF/B-V Multigroup Cross-Section Library for LMFBR Core and Shield, LWR Shield, Dosimetry, and Fusion Blanket Technology.* Oak Ridge, TN: Oak Ridge National Laboratory, report ORNL-5505.
9. Bartine, D. E., Knight, J. R., Pace, J. V., III, and Roussin, R., 1977. *Production and Testing of the DNA Few-Group Coupled Neutron-Gamma Cross-Section Library.* Oak Ridge, TN: Oak Ridge National Laboratory, report ORNL/TM-4840.
10. Rhoades, W. A., 1974. *Development of a Code System for Determining Radiation Protection of Armored Vehicles (The VCS Code).* Oak Ridge, TN: Oak Ridge National Laboratory, report ORNL/TM-4664.
11. Hashizume, T., Maruyama, T., Kumamoto, Y., Kato, Y., and Kawamura, S., 1969. Estimates of gamma-ray dose from neutron-induced radioactivity in Hiroshima and Nagasaki. Health Physics 17:761-771.
12. Pace, J. V., III and Kerr, G. D., 1984. Sulfur activation in electric pole insulators in Hiroshima. In *Second U.S.—Japan Joint Workshop for Reassessment of Atomic Bomb Radiation Dosimetry in Hiroshima and Nagasaki.* pp. 56-58. Hiroshima : Radiation Effects Research Foundation.
13. Straker E. A., Husar L., 1976. A Computer Code for the Prediction of Radiation, Blast, and Thermal Environments from Nuclear Weapons, Science Applications, Incorporated Report SAI-76-851-LJ.
14. Kerr, G. D., Pace, J. V., III, and Scott, W. H., Jr., 1983. Tissue Kerma vs distance relationships for initial nuclear radiation from the atomic bombs: Hiroshima and Nagasaki. In *U.S.—Japan Joint Workshop for Reassessment of Atomic Bomb Radiation Dosimetry in Hiroshima and Nagasaki,* pp. 57-103. Hiroshima: Radiation Effects Research Foundation.
15. Loewe, W. E., 1984. Radiation field associated with Hiroshima and Nagasaki. In *Reactor Dosimetry,* J. P. Denthon and H. Rottger, Eds., vol. 2, pp. 959-965. Dordrect, Holland: D. Reidel Publishing Co., European Communities report UEUR 9869.
16. Kerr, G. D. and Pace, J. V., III, 1985. Equations for total and partial densities of moist air. In *Report of Current Work of the Metabolism and Dosimetry Research Group, January 1, 1984-June 30, 1985,* pp. 74-77. Oak Ridge, TN: Oak Ridge National Laboratory, report ORNL/TM-9690.